actuators

Article

Minimum Cable Tensions and Tension Sensitivity for Long-Span Cable-Driven Camera Robots with Applications to Stability Analysis

Peng Liu [1,2,*], Haibo Tian [1] and Xinzhou Qiao [1]

[1] School of Mechanical Engineering, Xi'an University of Science and Technology, Xi'an 710054, China
[2] Key Laboratory of Ministry of Education for Electronic Equipment Structure Design, Xidian University, Xi'an 710000, China
* Correspondence: liupeng@xust.edu.cn

Abstract: Employing cables with strong flexibility and unidirectional restraints to operate a camera platform leads to stability issues for a camera robot with long-span cables considering the cable mass. Cable tensions, which are the constraints for the camera platform, have a critical influence on the stability of the robot. Consequently, this paper focuses on two special problems of minimum cable tension distributions (MCTDs) within the workspace and the cable tension sensitivity analysis (CTSA) for a camera robot by taking the cable mass into account, which can be used to investigate the stability of the robot. Firstly, three minimum cable tension distribution indices (MCTDIs) were proposed for the camera robot. An important matter is that the three proposed MCTDIs, which represent the weakest constraints for the camera platform, can be employed for investigating the stability of the robot. In addition, a specified minimum cable tension workspace (SMCTW) is introduced, where the minimum cable tension when the camera platform is located at arbitrary position meets the given requirement. Secondly, the CTSA model and cable tension sensitivity analysis index (CTSAI) for the camera robot were proposed with grey relational analysis method, in which the influence mechanism and influence degree of the positions of the camera platform relative to cable tensions was investigated in detail. Lastly, the reasonableness of the presented MCTDIs and the method for the CTSA with applications in the stability analysis of the camera robot were supported by performing some simulation studies.

Keywords: cable robot; camera robot; cable sag; minimum cable tension; sensitivity; stability

Citation: Liu, P.; Tian, H.; Qiao, X. Minimum Cable Tensions and Tension Sensitivity for Long-Span Cable-Driven Camera Robots with Applications to Stability Analysis. *Actuators* **2023**, *12*, 17. https://doi.org/10.3390/act12010017

Academic Editors: Bing Li, Wenfu Xu and Chenglong Fu

Received: 29 November 2022
Revised: 26 December 2022
Accepted: 29 December 2022
Published: 31 December 2022

1. Introduction

1.1. Background and Motivation

Cable robots, for which their end-effectors are operated using parallel cables, are a type of parallel robots; however, cable robots offer major advantages [1–4]. Therefore, cable robots have been employed in medical rehabilitation [5], 3D printing [6], wind tunnel experiments [7], astronomical observations [8], and other fields [9]. It is well known that cable robots are particularly suitable for large workspace manipulation tasks. Indeed, camera robots are redundant long-reach cable robots with a camera platform for implementing aerial camera tasks [10]; specifically, this paper focuses on camera robots. Employing cables, however, introduces numerous challenges for camera robots, of which the stability of the robot is the most critical concern. The employed cables can only apply tensile forces, so camera robots will become unstable when the cables lose their tension. Hence, the stability of camera robots is a major concern if cable tensions are less than the admissible values. Note that cable tensions, which are constraints for the camera platform, have critical influences on the stability of the robots. Therefore, not only the stability but also the cable tensions are important for camera robots. Meanwhile, the cable tensions vary relative to the positions of the camera platform. Small positional deviations in x, y, and

z directions may lead to sharp changes in the cable tensions, especially when the cable tensions are at the admissible upper and lower limits. The position deviations may lead to violation of the constraint conditions of cable tensions and even cause instability of the camera robot. This paper, in this regard, focuses on two special problems comprising minimum cable tension distributions (MCTDs) within the workspace and cable tension sensitivity analysis (CTSA) for the camera robots by taking the cable mass into account, which can be used to qualitatively investigate the stability of the robots. First, the usual straight cable assumption is irrational for camera robots. The influence of cable sags on camera robots must be handled for a camera robot that uses long-span cables [11]. Cable tensions, which have an important influence on the stability of camera robots, are affected by cable sags. The second most important factor is that the cable tensions strongly depend on the positions of the camera platform. Thus, the mechanism and degree of influence of the positions of the camera platform on cable tensions can be investigated by using the CTSA. Consequently, this paper mainly concentrates on the MCTDs and CTSA, with applications for stability analysis for camera robots.

1.2. Literature Review and Comments

In this section, we briefly review the literature that investigates cable tensions and their sensitivities relative to cable robots from two aspects. Firstly, we analyze the research studies that determine cable tensions and MCTDs for cable robots. Then, we review the body of literature related to the methods used CTSA relative to cable robots.

On the one hand, different methods have been employed to determine cable tensions for cable robots [12]. A method using convex theory to investigate cable tension was proposed in Ref. [13]. However, cable tension was solved using an iterative algorithm. A noniterative algorithm for obtaining continuous cable tensions is proposed in Ref. [14]. Cable tension was solved using the minimum 2-norm as the optimal objective in Ref. [15]. A noniterative algorithm using four optimal objective functions to determine cable tension was proposed in Ref. [16]. It is well known that a higher cable tension for cable robots is preferable due to higher stabilities under certain disturbances. In this case, a higher minimum cable tension can result in superior stabilities for cable robots. However, none of the aforementioned studies do consider the MCTDs within the workspace and their applications in investigating the stability of cable robots. Admittedly, when cable tension is a constraint of the camera platform, it has important influences on the stability of the cable robots, which can be employed to investigate the stability of cable robots. The MCTDs within the workspace for cable robots were investigated in Refs. [17,18]. Nevertheless, these proposed approaches for determining cable tensions for cable robots only considered massless straight line cables. It should be pointed that this assumption, for the camera robot with long-span cables, is irrational because of the sags observed in long-span cables [19,20]. Another important issue related to the cable tensions of camera robots is the cable model, i.e., the relationship between the shapes and tensions of the cables. Many works have examined the modeling of long-span cables, such as ideal straight line cables [21], elastic catenary cables [22], and nonelastic sagging cables [23]. It should be considered that the cable tension for a camera robot with non-negligible cable masses is quite different from that with straight-line cables. To the best of our knowledge, however, there are no findings in which the MCTDs, as well as the relationship between the stability of the robots and these MCTDs, investigate cable robots with long-span cables, such as camera robots.

Additionally, one of the most important issues in cable robots is that of the workspace [24,25]. Several different workspaces have been addressed previously, such as wrench-closure workspaces, wrench-feasible workspace, and so on. Particular importance will be attached to the fact that given such a minimum cable tension value, it is possible to construct a specified minimum cable tension workspace (SMCTW), which is the set of all positions of the cable robots where the minimum cable tension meets or exceeds the specified value. As a result, a useful workspace, the SMCTW, which can be defined as all positions where the camera platform can reach and operate effectively with specified stability, is presented.

An important advantage of the proposed SMCTW is that the specified stability for the cable robots can be guaranteed. This workspace is discussed in more detail. However, relatively little prior work exists in the area of the SMCTW for the camera robots with long-span cables.

On the other hand, cable tensions can be affected by many factors, such as factual pulley kinematics [26], cable-length variation and errors [27,28], and so on. Furthermore, the cable tension distribution sensitivity relative to the errors of cable tensions was investigated in Refs. [29,30]. The optimal methods for determining force sensitivity with respect to the structure matrix and twist vector of the 6-DOF cable-driven parallel robots were proposed by defining geometrical parameters related to the dimensions and configurations of the robot [31]. It is noted that cable tensions are affected by the positions of the camera platform, and moreover, the influence mechanism is complicated. Small position deviations in the x, y, and z directions may lead to sharp changes in the cable tensions, especially when the cable tensions are at the upper and lower limits. Consequently, this paper investigates cable tension sensitivity with regard to the positions of the camera platform; furthermore, the primary and secondary relationships between the positions of the camera platform and the cable tensions can be obtained. Moreover, by giving priority to the greater influencing factors for the cable tensions, the fluctuation in cable tensions and minimum cable tensions will reduce, ultimately contributing to the promotion and improvement of the stability for the camera robots. Meanwhile, the relationship between cable tensions and the positions of the camera platform cannot be established by functions. As a result, a major challenge to investigate the influence mechanism of the positions of the camera platform on the cable tensions that remains to be addressed is that only discrete numerical values of the cable tensions and the positions of the camera platform can be obtained. Actually, the influence mechanism of the above influencing factors on cable tensions for camera robots can be reflected using CTSA with the grey relational analysis method. Furthermore, their sequences can be ranked by the importance of each influencing factor [32]. Note that, to the knowledge of the authors, there a few findings that address the CTSA for cable robots. The stability sensitivity of cable robots was considered using the grey relational analysis method. Liu et al., in Ref. [33], proposed a method for quantitatively assessing the stability sensitivity for a cable-driven coal–gangue sorting robot, but the cables were modeled as ideal straight-line bodies for the investigated robot with a small workspace. Liu et al. presented a dynamic stability measurement method for high-speed long-span 4–1 cable robots. Moreover, a grey relational analysis method for dynamic stability was proposed to determine the primary and secondary relationships between the position and velocity of the end-effector, as well as the cable tension and the dynamic stability of the robots [34]. As a result, the grey relational analysis method can describe the relationships between the main factors and all other factors [35,36]. Therefore, it can be employed to obtain the sensitivity of each influencing factor and to rank their sequences. Several different models of grey relational analysis methods have been proposed based on the model proposed by Deng. Moreover, grey relational analysis has been widely applied to the prediction and control of the robots, decision making for the environmental system, and the influencing factors on the performance characteristics [37–41]. It should be pointed that complete data for the cable tensions and the positions of the camera platform cannot be obtained; thus, the results obtained from laws determining the relationships between them exhibited incomplete information. The grey system theory can be employed to address incomplete information and uncertain information [42,43]. For this reason, inspired by Refs. [33,34], the grey relational analysis method can be employed to investigate the CTSA for cable robots. As mentioned above, CTSA is a major concern for cable robots. Consequently, this paper aims to develop a method for CTSA relative to the camera robots, and a cable tension sensitivity analysis index (CTSAI) is presented using grey relational analysis. Furthermore, the CTSA for the camera robots can be employed to provide theoretical support for the promotion and improvement of the stability of the robot.

1.3. Contribution and Paper Organization

From above, the main focus of this paper is to investigate the MCTDs and CTSA, in addition to their applications to the stability of the camera robot while taking cable mass into account. The innovation of this paper, in detail, includes the following two aspects.

(i) Compared with Refs. [17,18], the objective of this paper, firstly, is to investigate the MCTDs within the workspace by taking the cable mass into account, which can be employed to qualitatively investigate the stability of the camera robot. In addition, the SMCTW, where the specified stability for the cable robots can be guaranteed, is proposed for the camera robots.

(ii) Secondly, inspired by Refs. [33,34], this paper proposes a CTSA method and CTSAI for camera robots with grey correlation analysis. However, there are few research studies on the methods for the CTSA of cable robots. With the CTSA, the primary and secondary relationship between the camera platform positions and cable tensions for the camera robots can be determined. Furthermore, by giving priority to greater influencing factors, the fluctuation of cable tensions and minimum cable tensions will reduce, ultimately contributing to the promotion and improvement of the stability of camera robots.

The remainder of this paper is structured as follows. The next section investigates the determination of cable tensions for a camera robot with long-span cables. The minimum cable tension when the camera platform is located at an arbitrary position within the workspace is determined; subsequently, three minimum cable tension distribution indices (MCTDIs) are developed to explain MCTDs within the workspace in Section 3. Section 4 proposes a method for the CTSA of the camera robots using grey correlation analysis. Moreover, several numerical examples are presented in Section 5. Finally, the conclusions and outlook are presented in Section 6.

2. Modeling of the Camera Robot with Long-Span Cables

Cables are pivotal for cable robots and thus, cable models have significant influences on the kineto-static analysis and the determining of cable tensions for cable robots. In fact, it has been known that long-span cables will tend to sag under their own weight, and moreover, the deviation from ideal massless cable model is significant and therefore cannot be ignored. Indeed, an inextensible catenary can be employed to express the cables for the long-span cable robots [44–46]. As a result, considering cable mass, a catenary equation is established in this section.

2.1. Catenary Equation of a Cable

Cable models comprise the key basis for obtaining cable tensions for a camera robot with long-span cables. The static sagging cable model, in this section, is introduced for the camera robot. Compared with the massless straight line model, the proposed cable model considering both cable mass and sag is more accurate for describing the cable behavior of the camera robot. The complete development of the equations of the static sagging cable can be found in Refs. [34,47]. The selected sagging cable model has higher accuracies than the ideal straight-line cable model and exhibits less complexity than the elastic catenary cable model. As a result, a brief overview of the catenary models of the long-span cables is presented in this section. As shown in Figure 1, a local cable frame $\{o_i{}^c x_i{}^c z_i{}^c\}$ is fixed to $\boldsymbol{B}_i$, where the z^c axis of the local cable frame coincides with the z axis of the base reference frame. As a consequence, the cable profile is catenary in nature; moreover, the catenary cable can be described as follows:

$$z_i^c = \frac{H_i}{\rho g}\left[\cosh \alpha_i - \cosh\left(\frac{2\beta_i x_i^c}{l_i} - \alpha_i\right)\right] \tag{1}$$

where ρ is the linear density of the catenary cable; g = 9.8 m/s^2 and is the gravitational acceleration; $\alpha_i = \sinh^{-1}\left[\frac{\beta_i(c_i/l_i)}{\sinh\beta_i}\right] + \beta_i$, $\beta_i = \frac{\rho g l_i}{2H_i}$; H_i and V_i are the horizontal and vertical components of the cable tension at the terminal point of the cable; l_i and c_i are the horizontal and vertical spans of the catenary cable, respectively.

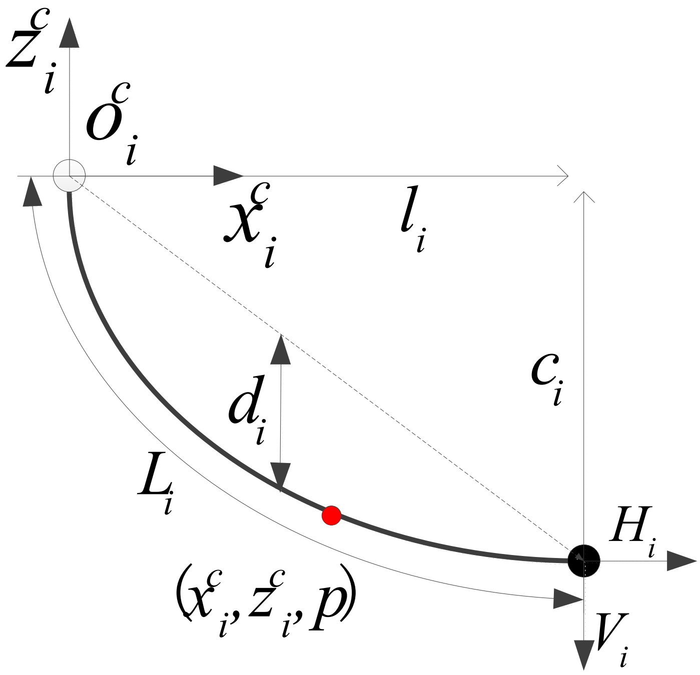

Figure 1. Catenary cable profile.

Then, the slope of catenary cable at the terminal point, the catenary cable length, L_i, and the corresponding sag, d_i, can be obtained according to the following equations, respectively.

$$\tan\gamma_i = \frac{\partial z^c{}_i}{\partial x^c{}_i} = \frac{-2\beta_i H_i}{\rho g l_i}\sinh(\frac{2\beta_i x^c{}_i}{l_i} - \alpha_i) \tag{2}$$

$$L_i = \sqrt{1 + \left(\frac{\mathrm{d}z_i^s}{dx_i^s}\right)^2} = l - \frac{H\beta}{ql}\left[\frac{l}{16\beta}\left(e^{4\beta-2\alpha} - e^{-4\beta+2\alpha}\right) + \frac{1}{2}\right] \tag{3}$$

$$d_i = \frac{8H_i \sinh\beta_i \sinh^{-1}\left(\frac{\rho g c_i/2H_i}{\sinh\beta_i}\right) - c_i\rho g}{2\rho g} \tag{4}$$

Observing Equation (4), the cable sag highly depends on the horizontal component H_i. In fact, the sag-to-span ratio, which denotes the ratio of the sag to span for the catenary cable, will be introduced in Section 2.3. It must be as small as possible to keep the cables under tension [34].

2.2. Modeling the Camera Robot

Note that in the catenary cable model, the profile of the cable highly depends on cable tensions. That is to say, that there is an interaction between the kinematics and statics of the camera robot. Meanwhile, there are multiple solutions to the kineto-static problem for the camera robot; thus, a method for obtaining a unique solution to the kineto-static problem with a selection criterion must be proposed, which is investigated in Section 2.3.

As shown in Figure 2, the camera is installed on the camera platform. The three translational DOFs of the camera are accomplished by the four cables, while the three rotational DOFs of the camera are achieved by the camera platform with a composite hinge structure. Indeed, by means of a composite hinge structure, the decoupling of the translation and rotation for the camera can be achieved, so the camera platform can be seen as an ideal mass point. As a result, the camera robot consists of a camera platform with three translational motions in the x, y, and z directions driven by four cables. It should be noted that the camera robot is a redundantly actuated cable-driven parallel robot, and it is different from underactuated cable-driven parallel robots [48]. Thus, the orientations of the camera do not introduce inertial forces or influence the cable tension distributions and equilibrium of the camera robot. In more detail, the camera robot comprises mechanical and control modules. The mechanical module consists of a fixed frame, four cable drive units, and a mobile camera platform, while the control module composes of an IPC, motion controllers, encoders, and so on. In addition, a laser tracker is equipped for measuring the positions of the camera platform. In more detail, the control signals can be generated with IPC and motion control cards and can be transmitted to the servo drivers. The coordinated movement of the four cables leads to the desired camera platform movement, which can then realize mobile photographs. The positions of the camera platform are measured with a laser tracker, while the four cable lengths are computed with the data collected with the encoders. The cable tensions are obtained by a few meters. These collected data are fed back to the IPC, which can realize the closed-loop control of the camera robot. Furthermore, a base reference frame, noted as $OXYZ$, is attached to the fixed base, where O is the origin point. $\boldsymbol{p} = (x, y, z)^{\mathrm{T}}$ is a position vector representing the position of the camera platform in $OXYZ$. Point B_i, at which the ith cable (i = 1, 2, 3, 4) enters the pulley, is assumed to be fixed to the base frame.

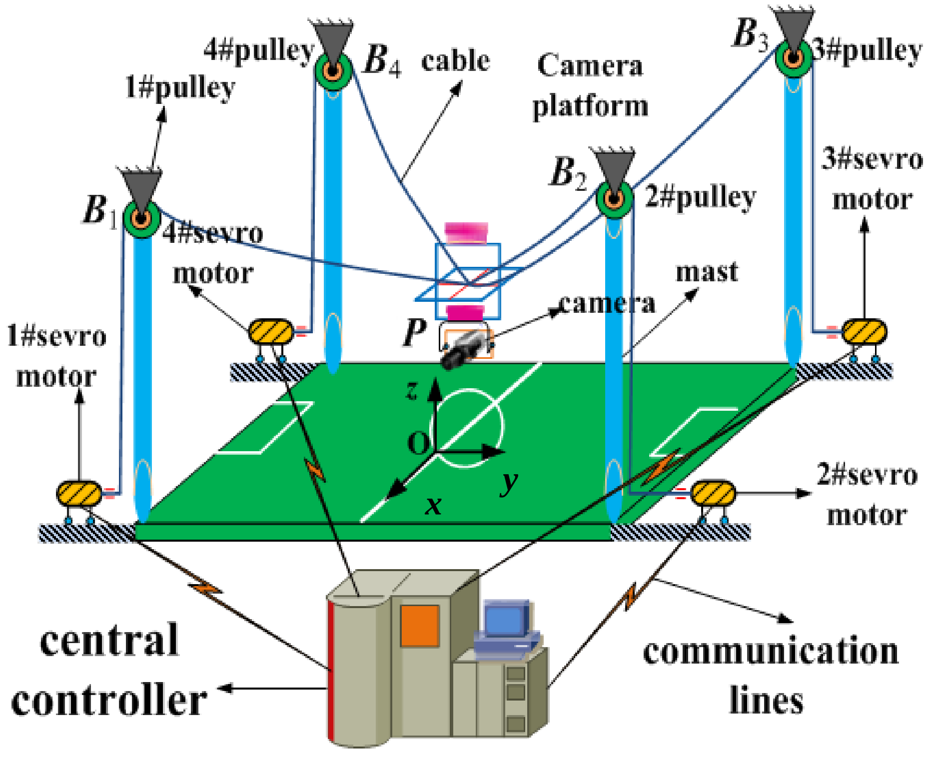

Figure 2. Schematic of a camera robot.

Indeed, contrary to the massless straight line cables, the cable tensions change relative to the catenary cables. In particular, the cable tension $\boldsymbol{T}_i$ at the last node, $\boldsymbol{p}$, can be represented in terms of $\boldsymbol{T}_i = [H_i\cos\theta_i\ H_i\sin\theta_i\ H_i\tan\gamma_i]^{\mathrm{T}}$. θ_i is the angle between the x^{s} axis of $o^{\mathrm{c}}x^{\mathrm{c}}z^{\mathrm{c}}$ and the x axis of $OXYZ$: $V_i = H_i\tan\gamma_i$. The cable tension $\boldsymbol{T}_i$ can be decomposed into the three directions of the coordinate axis of $OXYZ$ at the last node $\boldsymbol{p}$. Moreover, the kineto-static equation of the camera robot can be expressed as follows.

$$\begin{cases} \sum_{i=1}^{4} H_i \cos\theta_i + f_{e,x} = 0 \\ \sum_{i=1}^{4} H_i \sin\theta_i + f_{e,y} = 0 \\ \sum_{i=1}^{4} H_i \tan\gamma_i - \sum_{i=1}^{4} \rho g L_i - m_p g + f_{e,z} = 0 \end{cases} \tag{5}$$

For the sake of simplicity, Equation (5) can be presented with a matrix form as follows:

$$\boldsymbol{J}\boldsymbol{H} - \boldsymbol{f}_g - \boldsymbol{f}_G + \boldsymbol{f}_e = 0 \tag{6}$$

where mp is the camera platform mass; $m_c = \rho \sum_{i=1}^{4} L_i$ is the total mass of the four cables; $\boldsymbol{H} = [H_1 \quad H_2 \quad H_3 \quad H_4]^T$ is the horizontal components of the four cable tensions at the last node p; $\boldsymbol{f}_g = m_c g = \rho g \sum_{i=1}^{4} L_i$ is the gravitational force of cables; $\boldsymbol{f}_G = [0\ 0\ m_p g]^T$ is the gravitational force of the camera platform; and $\boldsymbol{f}_e = [f_{e,x}\ f_{e,y}\ f_{e,z}]^T$ denotes the external forces. Furthermore, Equation (6) can be expressed as follows:

$$\boldsymbol{J}\boldsymbol{H} = \boldsymbol{Q} \tag{7}$$

where $\boldsymbol{Q} = \boldsymbol{f}_g + \boldsymbol{f}_G - \boldsymbol{f}_e$, $\boldsymbol{J} = [J_1\ J_2\ J_3\ J_4]$ is the structure matrix and $J_i = [\cos\theta_i\ \ \sin\theta_i\ \ \tan\gamma_i]^{\mathrm{T}}$ (i = 1,2,3,4).

2.3. Optimal Model for Cable Tensions

Cables have unilateral driving properties, so the camera robot must be manipulated redundantly. Since the camera robot with a redundant drive is taken into consideration in this paper, there may be infinite solutions to vector $\boldsymbol{H}$. According to matrix theory, vector $\boldsymbol{H}$ can be obtained using the following formula [49]:

$$\boldsymbol{H} = (\boldsymbol{J}(\boldsymbol{H}))^{+} \boldsymbol{Q}(\boldsymbol{H}) + \boldsymbol{N}(\boldsymbol{J}(\boldsymbol{H}))\lambda \tag{8}$$

where $\boldsymbol{J}^{+}\boldsymbol{Q}$ and $\boldsymbol{N}(\boldsymbol{J})\lambda$ are the special solution and homogeneous solution to vector $\boldsymbol{H}$, respectively, in which $\boldsymbol{N}(\boldsymbol{J})$ is the kernel of matrix $\boldsymbol{J}$, and λ is an arbitrary scalar.

The vertical component of the tension at the terminal point of cable i can be represented as follows.

$$V_i = H_i \tan\gamma_i (i = 1, 2, 3, 4) \tag{9}$$

As a result, the cable tension, based on Equation (9), can be obtained using the following formula.

$$T_i = H_i \sqrt{1 + \tan^2\gamma_i} (i = 1, 2, 3, 4) \tag{10}$$

Note that the following conditions must be met for the cable tension $\boldsymbol{T}$ to keep the cables under tension:

$$\boldsymbol{T}_{\mathrm{s,min}} \leq \boldsymbol{T} \leq \boldsymbol{T}_{\mathrm{s,max}} \tag{11}$$

where $\boldsymbol{T}$ = $[T_1, T_2, T_3, T_4]^{\mathrm{T}}$ is the vector consisting of all the four cable tensions; $\boldsymbol{T}_{\mathrm{s,min}}$ is the lower boundary of the cable tension and $\boldsymbol{T}_{\mathrm{s,max}}$ is the upper boundary of the cable tension.

Apart from the above, keeping the cables as taut as possible normally leads to work for the camera robot. In other words, making the sag-to-span ratio r_i agree with the predetermined condition, as mentioned above, is required in actual practice. Moreover, it can be expressed as follows:

$$r_i = \frac{|d_i|}{l_i} \times 100\% \leq r_{i,\max} \tag{12}$$

Furthermore, combining Equations (8)–(12) leads to the following expression:

$$\lambda \in [\underline{\lambda}, \overline{\lambda}] \tag{13}$$

where $\underline{\lambda}$ is the lower boundary of λ and $\overline{\lambda}$ is the upper boundary.

It should be pointed that there are multiple solutions to Equation (8); therefore, the minimum variance is employed to obtain a unique solution using Equations (7) and (13) as the constraint conditions. Consequently, the vector $\boldsymbol{H}$ can be obtained by the following optimization model:

$$\begin{array}{cc} Object & f(\lambda) = min\left(\frac{1}{4}\left[\sum\limits_{i=1}^{4}(H_i - E(\boldsymbol{H}))^2\right]\right) \\ subject\ to & \boldsymbol{JH} = \boldsymbol{Q} \\ & \underline{\lambda} \leq \lambda \leq \overline{\lambda} \end{array} \tag{14}$$

where $E(\boldsymbol{H})$ is the arithmetic mean value of the vector $\boldsymbol{H}$.

3. MCTDs with Applications to Stability Analysis

In this section, we will exhibit a method for investigating MCTDs and their applications for investigating the stability of the camera robot. It is well known that with regard to the camera robot, employing cables with strong flexibility and unidirectional restraint leads to a stability issue. It should be noted that the proposed stability of the camera robot indicates the robustness against external interferences while the camera platform is in equilibrium. In fact, the camera platform will be disturbed along the weakest constraint direction. Therefore, the proposed stability of the camera robot is the structural stability of equilibrium. Moreover, the stability of the camera robot is similar to the equilibrium stability of the free motion for the underactuated cable-driven parallel robots [50]; however, it is different from the stability of a controller [51]. As a result, the stability is able to resist external disturbances at the weakest constraint direction, namely, the cable direction with minimum cable tensions (MCTs); therefore, MCTs can be employed to investigate the stability for the camera robot. Meanwhile, the presented stability of the camera robot is similar to the one of the compressive bar system, where the instability of the compressive bar system occurs when the pressure of the weakest bar is larger than a certain value [52]. Similarly, with regard to the camera robot, the cable possessing MCTs when the camera platform is located at an arbitrary equilibrium position will slacken when the MCTs are less than a certain value, resulting in the missing ability to constrain the camera platform for the camera robot. One important similarity between the two problems is that the presented stability for the two systems highly depends on the weakest constraint. Therefore, in order to obtain more information about the MCTDs in a specified region of the workspace, three minimum cable tension distribution indices (MCTDIs) are proposed, which, as mentioned above, can be employed to investigate the stability of the camera robot.

3.1. Three Minimum Cable Tension Distribution Indices (MCTDIs)

As observed above, the vector $\boldsymbol{H}$ can be obtained from Equation (14) by using an iterative optimization model with a highly nonlinear Equation (7). At the same time, cable tension $\boldsymbol{T}$ can be calculated with Equation (10). It should be pointed out that the cable tension $\boldsymbol{T}$ strongly depends on the positions of the camera platform. Furthermore, the MCTs when the camera platform is located at an arbitrary position of the workspace can be obtained while cable tension vector $\boldsymbol{T}$ is determined using Equation (14). As a result, the

MCTs also depend on the positions of the camera platform, and the MCTs can be obtained using the following formula:

$$T_{min}(\boldsymbol{X}) = min(\boldsymbol{T}(\boldsymbol{X})) \tag{15}$$

where $min(\bullet)$ is the smallest element in vector $\boldsymbol{T}$ and $\boldsymbol{X}$ represents the position of the camera platform.

As stated previously, MCTs can be employed to investigate the stability of the camera robot. As a result, three MCTDIs, which show MCTDs in some regions of the workspace, are proposed. The three MCTDIs are denoted by $\Re_V$, $\Re_H$, and $\Re_A$ respectively, in which $\Re_V$ and $\Re_H$ represent the MCTDs on the vertical midline and on the planes that are parallel with the horizontal plane, respectively; furthermore, $\Re_A$ is presented to depict the comprehensive MCTDs within the entire workspace. The three proposed MCTDIs can be defined as follows:

$$\Re_V = \frac{T_{vsp,min}}{T_{top,min}} \tag{16}$$

$$\Re_H = \frac{T_{wsp,min}}{T_{cp,min}} \tag{17}$$

$$\Re_A = \Re_V \times \Re_H \tag{18}$$

where $T_{vsp,min}$ is the MCT when the camera platform is located at an arbitrary specified position of the vertical midline of the workspace; $T_{top,min}$ is the MCT when the camera platform is located at the top of the vertical midline; $T_{wsp,min}$ is the MCT when the camera platform is located at an arbitrary specified position; $T_{cp,min}$ is the MCT when the camera platform is located at the central position of the horizontal plane, which the specified position is within. Therefore, the MCTDs over the entire workspace can be described with the proposed three MCTDIs.

In more detail, since increasing the elevation of the camera platform position leads to an increase in the angles between T_i and V_i, cable tensions have to increase to counteract the gravitational force of the camera platform. Thus, the numerators of the three MCTDIs are all less than their denominators, and therefore, preference will be given to the fact that the values of the three MCTDIs lay between 0 and 1 without exception, which can be used advantageously to construct the stability index in the further research.

3.2. SMCTW Generation Algorithm

One of the most important issues in cable robots is that of the workspace. A useful workspace, the specified minimum cable tension workspace (SMCTW), is proposed in this section, and it comprises all positions at which the camera platform is located at and all cables that have specified MCTs; therefore, it can meet the predetermined stability requirements. As a result, the SMCTW can be employed to provide theoretical support for the motion trajectory design of the camera platform for a camera robot. With the definition of the SMCTW, the generation algorithm for the SMCTW can be expressed as follows:

(1) Input the position of the camera platform, $\boldsymbol{X}_i$ (i = 1, 2, . . . , N. N is the total number of positions); the MCT limit $T^*{}_{min}$; external wrench $\boldsymbol{f}_e(\boldsymbol{X}_i)$; and the gravity of the camera platform, $\boldsymbol{f}_g(\boldsymbol{X}_i)$.
(2) Determine the horizontal component of the cable tension, $\boldsymbol{H}$, with Equation(14) using the convex programming theory.
(3) Obtain cable tension vector $\boldsymbol{T}$ using Equation (9) and Equation (10).
(4) Calculate the $\boldsymbol{T}_{min}(\boldsymbol{X}_i)$ with Equation (15).
(5) Judge whether $\boldsymbol{T}_{min}(\boldsymbol{X}_i)$ exceeds $T^*{}_{min}$. If it does, record and output the position of camera platform $\boldsymbol{X}_i$; if not, proceed to the next position.
(6) Judge whether $\boldsymbol{X}_i$ is the last position of the camera platform within the workspace. If not, proceed to step (1) and solve $\boldsymbol{T}^*(\boldsymbol{X}_{i+1})$ and $\boldsymbol{T}_{min}(\boldsymbol{X}_{i+1})$ for the next position, $\boldsymbol{X}_{i+1}$; if it is, record and output position $\boldsymbol{X}_i$ and stop.

4. Grey Relational Analysis Method for the CTSA

As mentioned before, cable tensions and the MCTs highly depend on the positions of the camera platform. Moreover, the influence laws of the positions of the camera platform on the cable tensions are investigated to determine the primary and secondary relationship between the positions of the camera platform and cable tensions for the camera robots. By giving priority to the greater influencing factor relative to the cable tensions, the fluctuation of cable tensions and minimum cable tensions will reduce, ultimately contributing to the promotion and improvement of the stability of camera robots. As a result, this section is primarily with the influencing degree of the positions of the camera platform on the cable tensions for the camera robots. Additionally, note that the importance of these influencing factors on the cable tensions can be evaluated by using the CTSA. The CTSA for the camera robots is used to quantitatively investigate the influencing degree of the influencing factors on the cable tensions. The greater sensitivity the influencing factor on the cable tensions relative to the camera robots, the greater the influence on the cable tensions and vice versa. Therefore, via the CTSA, the most sensitive influencing factor relative to the cable tensions can be identified and prioritized for the camera robots. As a result, a grey relational analysis method for CTSA is developed in this section. In detail, the proposed grey relational analysis method for the CTSA can be described by using the following four steps [53–55].

(1) Determination of the cable tensions and influencing factor sequences

According to the grey correlation theory, the values of cable tensions for the camera robots, in this section, are set as the reference sequence; meanwhile, the positions of the camera platform (the displacement component of the x-axis, y-axis, and z-axis) are set as the comparison sequences. We suppose that the reference and comparable sequences are, respectively, denoted as $\boldsymbol{G}_0 = [G_0(1), G_0(2), \cdots, G_0(k)]^T$ and $\boldsymbol{G}_i = [G_i(1), G_i(2), \cdots, G_i(k)]^T$, $i = 1, 2, 3$, where i is number of influencing factors for the cable tensions; moreover, k is the changing number of the cable tensions and their influencing factors for the camera robots. Therefore, the entire sequence matrix for the CTSA of the camera robots is comprised two crucial sequences, and it can be defined as follows.

$$\boldsymbol{G} = \begin{bmatrix} G_0(1) & G_1(1) & G_2(1) & G_3(1) \\ G_0(2) & G_1(2) & G_2(2) & G_3(2) \\ \cdots & \cdots & \cdots & \cdots \\ G_0(k) & G_1(k) & G_2(k) & G_3(k) \end{bmatrix} \tag{19}$$

(2) Normalization of the sequence matrixes

In general, the raw data of the cable tension reference sequence and the influencing factor comparison sequence may differ from the others in terms of their range and their measurement units; thus, the influence of some factors may be neglected. As a result, this leads to an incomparable condition and even incorrect conclusion. As a result, the main procedure of the grey relational analysis for the CTSA of the camera robots is firstly a normalization treatment on the initial data of the sequence matrixes to obtain the grey correlation grades. Furthermore, these sequences can be transformed with the following formula.

$$G_l{}'(j) = \frac{G_l(j) - \min G_l(j)}{\max G_l(j) - \min G_l(j)}, (l = 0, 1, 2, 3; j = 1, 2, \cdots, k) \tag{20}$$

(3) Grey correlation coefficient

After the normalization treatment for the sequence matrixes, the absolute difference between the cable tension reference sequence and each influencing factor comparison sequence, denoted by $\Theta_{0i} = |G_0(j) - G_i(j)|$, can be obtained. Moreover, the maximum difference denoted by $\Theta_{\max} = \max\limits_{1 \le i \le 3} \max\limits_{1 \le j \le k} |G_0(j) - G_i(j)|$ and the minimum difference denoted by $\Theta_{\min} = \min_{1 \le i \le 3} \min_{1 \le j \le k} |G_0(j) - G_i(j)|$ can be obtained. Therefore, the grey relation coefficients can be obtained as follows:

$$r_{ij}(j) = \frac{\Theta_{\min} + \varpi\Theta_{\max}}{\Theta_{0i}(j) + \varpi\Theta_{\max}} \tag{21}$$

where ϖ is the distinguishing coefficient; the distinguishing coefficient is set as 0.5 in this paper.

(4) Grey relational CTSAI

The correlation between the cable tension reference sequence and influencing factor compared sequences can be represented by the grey relational degree. As a result, if a certain influencing factor in the compared sequence is far more critical than other influencing factors to the cable tensions, the obtained grey correlation degree of the influencing factor will be higher than other grey correlation degrees. As a result, the grey correlation degree, in this paper, is employed to measure the influence degree of camera platform positions on cable tensions for the camera robots. Main factors and secondary influencing factors, and the maximum and minimum influencing factors for the cable tensions of the camera robots, can be obtained through the influencing factor correlation degrees. From the above, a grey correlation analysis method for CTSA is proposed and measured with the grey correlation degree in this section; hence, the CTSAI for the camera robots, after deriving the grey relational coefficients, can be obtained as follows:

$$CTSAI_i = \frac{1}{k}\sum_{j=1}^{k} r_{ij}(j) \tag{22}$$

It is worth noting that three CTSAIs can be obtained for the camera robots, and they denote the influence degree of the displacement component of x-axis, y-axis, and z-axis for the camera platform on the cable tensions, respectively. Therefore, the three CTSAIs can be employed to obtain the sensitivity of the camera platform positions on cable tensions and rank their sequence.

5. Results and Discussion

5.1. MCTDIs and Their Application

The MCTs among the four cables, the proposed MCTDIs, and their applications for investigating the stability of the robot are supported by performing some simulation studies on a camera robot. And furthermore, the parameters of the used camera robot are shown in Table 1.

Table 1. Parameters of the camera robot.

Parameters of the Robot	Symbol	Values
Cable diameter	d	0.15 cm
Cable linear density	ρ	0.1851 kg/m
Camera platform mass	m_p	20 kg
Lower boundary of $\boldsymbol{T}$	$T_{\min}$	100 N
Upper boundary of $\boldsymbol{T}$	$T_{\max}$	10000 N
Position of the 1st pulley (Figure 2)	$\boldsymbol{B}_1$	$(0,0,23)^{\mathrm{T}}$ m
Position of the 2nd pulley	$\boldsymbol{B}_2$	$(100,0,23)^{\mathrm{T}}$ m
Position of the 3rd pulley	$\boldsymbol{B}_3$	$(100,90,23)^{\mathrm{T}}$ m
Position of the 4th pulley	$\boldsymbol{B}_4$	$(0,90,23)^{\mathrm{T}}$ m

The MCTs while the camera platform is located on different vertical planes within the workspace are depicted in Figure 3, where "red +", "blue +", "green", "red", and "blue –" represent "800 N <= MCT <= 900 N", "900 N <= MCT <= 1000 N", "1000 N <= MCT <= 2000 N", "2000 N <= MCT <= 3000 N", and "3000 N <= MCT <= 5000 N", respectively. As observed, the interior scopes where the camera platform is located at can hold larger MCTs than the external scopes. It should be noted that Figure 3a,b show a section of the SMCTW for the camera robot, respectively. As expected, further insights into the integral shape of the SMCTW can be obtained from Figure 3. It is evident that the change laws of MCT while the camera platform locates on the middle vertical plane YOZ with x = 50 m and on the middle vertical plane XOZ with y = 45 m, which is that the upper-middle positions where the camera platform locates possess bigger MCTs than the ones around them, are consistent with each other. This is because the redundant cable tensions are distributed more evenly among the four cables when the camera platform is located at the center positions, and while the cable tensions are greater as the γ decreases to balance the gravity of the camera platform when it is located at the upper positions of the workspace. It is indicated in Figure 3a,b that MCTs on the horizontal plane of the workspace are a series of elliptical equipotential lines, and it should be noted that these results are consistent with the conclusion of Ref. [17]. From the results, it has been depicted that the four cable tensions relative to the catenary cables are far greater than the cable tensions observed relative to the massless straight-line cables in Ref. [17] for the camera robot. The direction of the MCTs, as a matter of fact, is the weakest constraint direction when the camera platform is located at the present position for the camera robot. The proposed stability of the robot reflects the fact that the camera platform did not depart from the present position along the weakest constraint direction while external disturbances are on. Hence, the MCTs can increase the constraint of the weakest direction, further improving the stability of the camera robot.

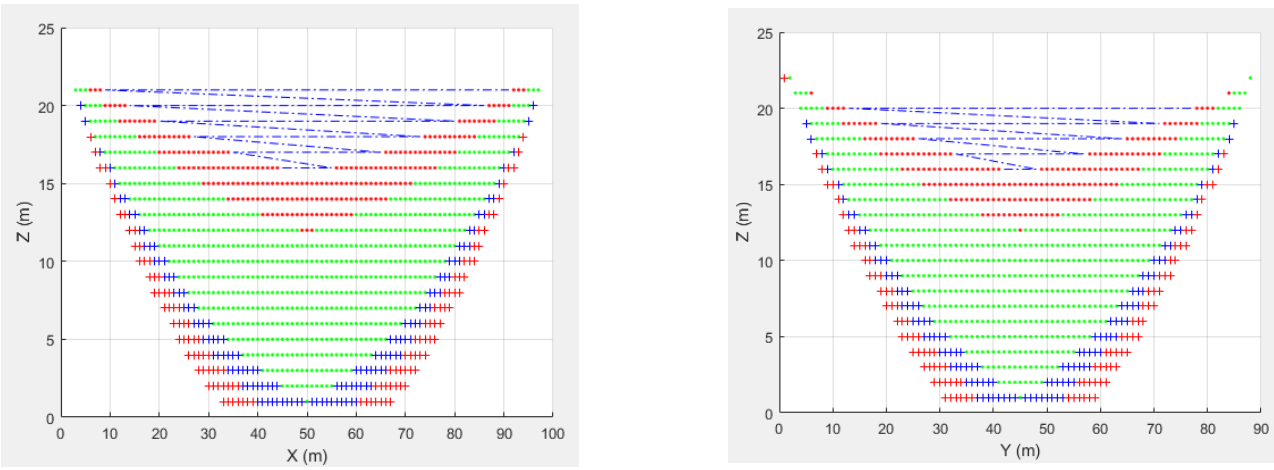

(**a**) (**b**)

Figure 3. MCTs on the workspace sections: (**a**) MCTs on the plane y = 45 m, (**b**) MCTs on the plane x = 50 m.

The proposed MCTDIs are obtained for the camera robot based on MCTs, and MCTDI $\Re_A$ on the plane y = 45 m and $\Re_A$ on the plane x = 50 m are displayed in Figure 4a,b, respectively. Note that Figure 4a,b are the sections of the proposed MCTDIs within the workspace, respectively. Moreover, further insight into the integral shape of MCTDIs within the workspace can be obtained from Figure 4. As can be seen from Figure 4, the obtained results for the MCTDI, which are in the interval [0,1], are a set of equipotential lines. Further, the MCTDIs while the camera platform is located on the upper-middle area of the workspace are bigger than the ones outside, and this is because the positions where the camera platform is located at hold bigger MCTs due to the uniformity of the four cable tensions. As a result, the MCTs are larger than others while the camera platform is located on the upper-middle area of the workspace, thereby holding stronger constraints for the camera platform. From above, it was obvious that the MCTs and the proposed MCTDIs, which represent the weakest constraints for the camera platform, can be employed to investigate the stability of the camera robots.

5.2. CTSA for the Camera Robot

As shown in Figure 5, the Cartesian trajectory of the camera platform for the camera robot is selected to investigate the effects of the long-span cables on cable tensions and the MCTs and the proposed CTSA method, and the spatial spiral is defined by the following equation:

$$\begin{cases} x = R\cos(\omega t) + 50 \\ y = R\sin(\omega t) + 45 \\ z = vt + 10 \end{cases} \tag{23}$$

where R = 10 m; ω = 0.2π rad/s; v = 1 m/s; the starting and ending positions of the trajectory are $(60, 45, 0)^{\mathrm{T}}$m and $(60, 45, 10)^{\mathrm{T}}$m, respectively.

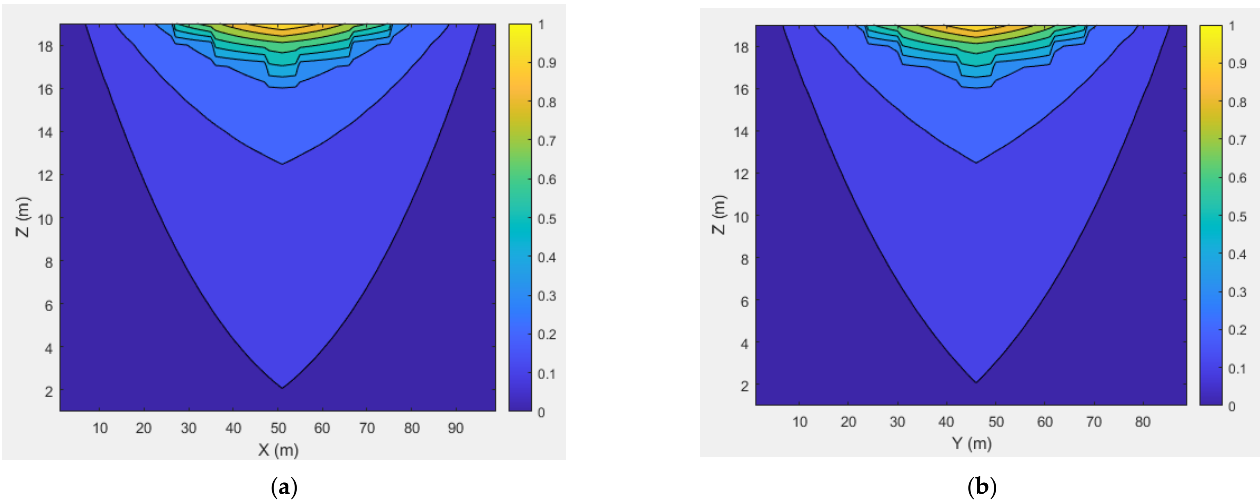

Figure 4. MCTDIs within the workspace: (**a**) $\Re_A$ on the plane y = 45 m, (**b**) $\Re_A$ on the plane x = 50 m.

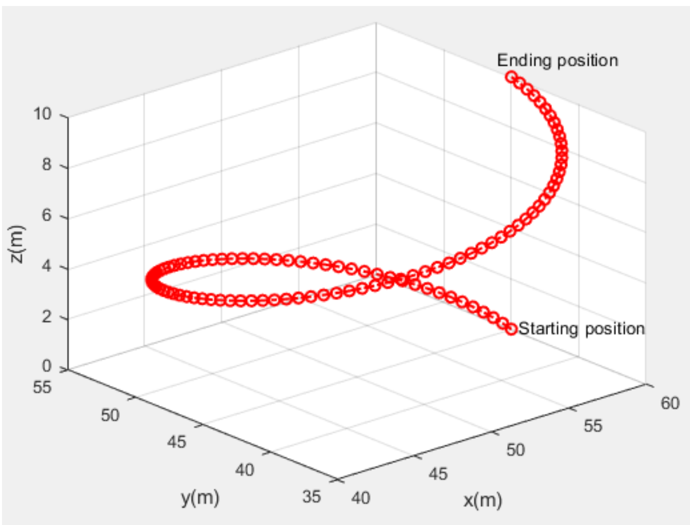

Figure 5. A spatial spiral trajectory for a camera robot.

Firstly, the cable tensions of the four cables along the spatial spiral trajectory with the two models are shown in Figure 6. As can be seen clearly in the figure, the cable tensions computed by the catenary cables are quite different the ones obtained by the massless straight-line cables. In detail, it can be seen that cable tensions with the catenary cables are about four times that of the straight-line cable model. It should be pointed that the cable tensions obtained by the two cable models are smooth and continuous, and there will not be an impact on the motion of the camera robot. Therefore, cable sags must be considered for the camera robot.

Moreover, the influence degrees of the displacement component of the x-axis, y-axis, and z-axis for the camera platform relative to the four cable tensions and the MCTs are investigated in this section. As previously indicated, cable tensions highly depend on the positions of the camera platform; however, the relationship between the cable tensions and the positions cannot be described by functions. Thus, only the discrete numerical values of cable tensions and the positions of the camera platform can be obtained by simulations. One hundred sets of data about the positions of the camera platform and cable tensions for the camera robot are obtained by simulation, and ten groups of the obtained data used to perform approximate treatments are displayed in Table 2. Note that the presented data about the z-axis displacement of the camera platform increase with equal differences, and this is because the data were obtained by simulations using the equal step method.

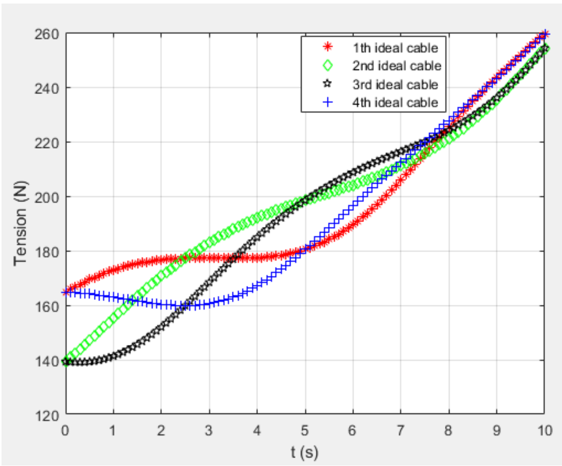

(**a**)

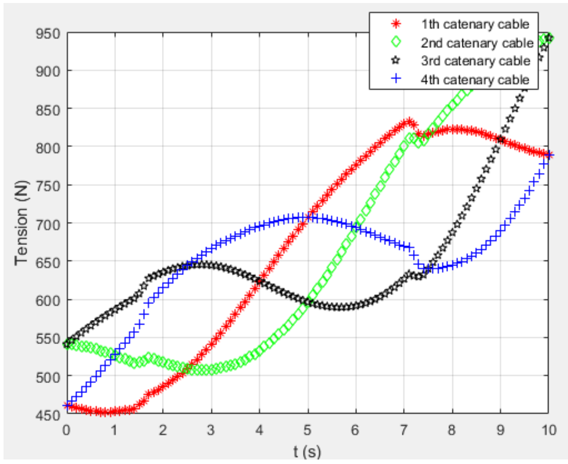

(**b**)

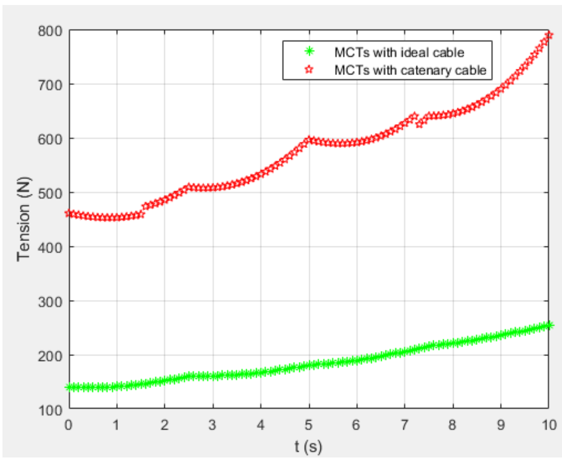

(**c**)

Figure 6. Cable tension with catenary and ideal cables: (**a**) cable tension with the ideal cables, (**b**) cable tension with the catenary cables, (**c**) MCTs with two cable models.

Table 2. Original data of cable tensions and positions of the camera platform.

Reference Sequence					Comparison Sequence		
T_1(N)	T_2(N)	T_1(N)	T_2(N)	MCT(N)	x(m)	y(m)	z(m)
452.62	528.83	582.42	520.28	452.62	58.44	50.36	0.90
481.88	519.25	633.01	608.57	481.88	53.68	54.29	1.90
534.19	507.44	645.20	662.41	507.44	47.51	54.69	2.90
614.48	528.63	626.58	693.52	528.63	42.29	51.37	3.90
699.21	588.35	598.51	706.93	588.35	40.02	45.63	4.90
769.86	683.04	590.52	696.08	590.52	41.55	39.64	5.90
824.96	790.47	621.04	671.51	621.04	46.32	35.70	6.90
822.35	847.07	677.02	642.85	642.85	52.48	35.31	7.90
811.18	905.51	796.33	683.10	683.10	57.71	38.62	8.90
790.25	940.47	929.47	776.78	776.78	59.98	44.37	9.90

The point is that three CTSAIs for one cable tension can be calculated, and the sensitivity of each influencing factor can be obtained, therefore ranking their sequence. It should be pointed that there, as a result, will be fifteen CTSAIs for the four cable tensions and the MCTs altogether. Moreover, the original data for cable tensions and positions of the camera platform, which are shown in Table 2, are handled and the 15 CTSAIs can be obtained. Moreover, the results are displayed in Figure 7a,e while the distinguishing coefficient is set as 0.5. It is worth noting that the change laws of the obtained CTSAIs for the four cable tensions and MCTs consistent with each other. It is known that the CTSAI close to 1 means the influence degree of this factor to cable tensions of the camera robot is great. From the results in Figure 7, it has been depicted that the CTSAIs for the camera robot are greater than 0.5 for T_3, T_4, and MCT; hence, this indicates that the displacement components of the x-axis, y-axis, and z-axis for the camera platform have a key influence on for T_3, T_4, and the MCT. Note that the CTSAIs of x-axis and z-axis displacement of the camera platform are greater than 0.5 for T_1 and T_2, while the CTSAIs of y-axis are slightly less than 0.5. The obtained results for the CTSA of the camera robot show that with respect to the selected three influencing factors for the cable tensions, the importance is defined by the following sequence: z-direction displacement of the camera platform > x-axis displacement > y-axis displacement. The effects of the distinguishing coefficient on the CTSAI for the camera robot are investigated in detail; moreover, the CTSAI for the MCTs is depicted in Figure 7f when the distinguishing coefficient is set as 0.6. By observing the results, it is evident that the influence laws of the displacement component of the x-axis, y-axis, and z-axis for the camera platform on the MCTs, for different distinguishing coefficients, are consistent with each other.

From the above results, the y-axis displacement of the camera platform has the least amount of impact on the cable tensions and conversely, the z-axis displacement of the camera platform has an important impact on them. As a result, it is necessary to strictly control the motion accuracy of z-axis of the camera platform, which will reduce the fluctuation of cable tensions, ultimately contributing to the promotion and improvement of the stability for the camera robots.

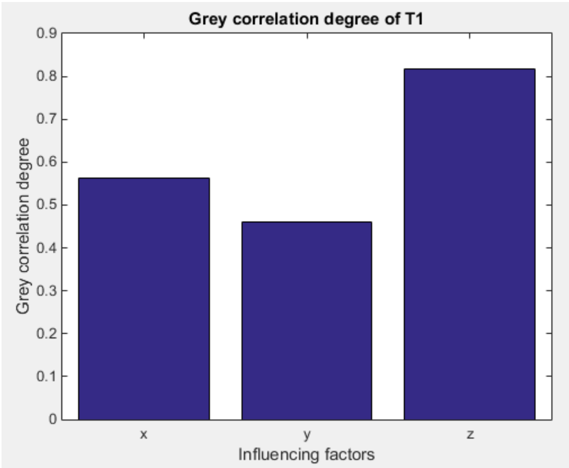

(**a**)

(**b**)

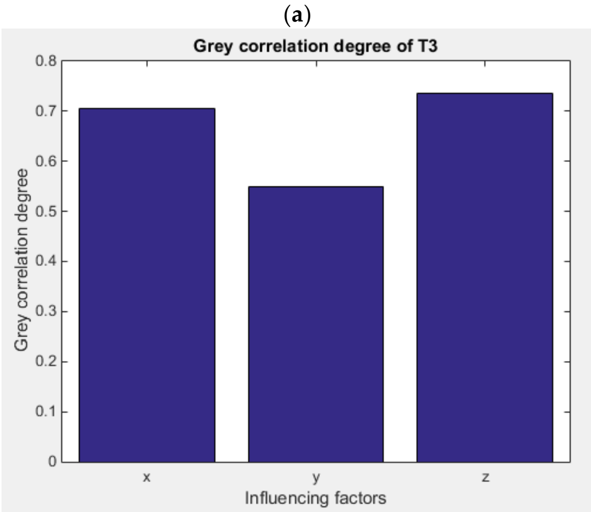

(c)

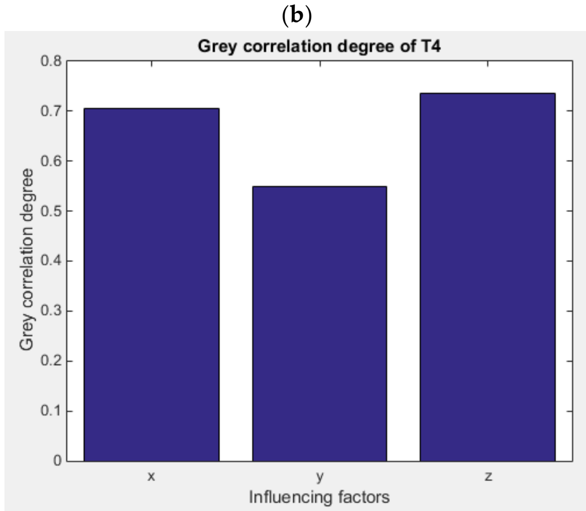

(**d**)

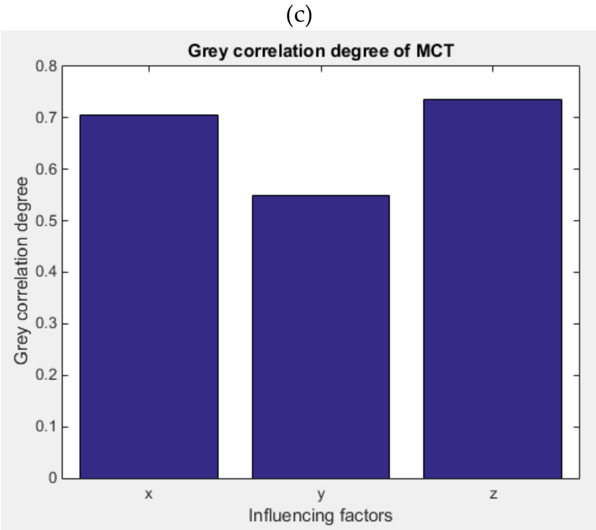

(**e**)

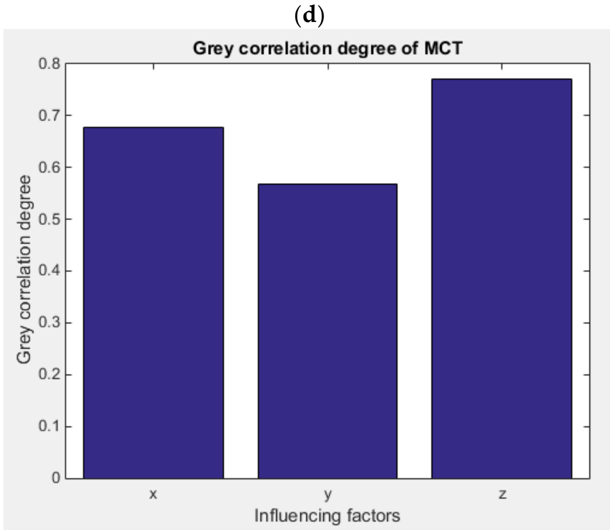

(**f**)

Figure 7. CTSAIs for camera robots: (**a**) grey correlation degree of T_1, (**b**) grey correlation degree of T_2; (**c**) grey correlation degree of T_3, (**d**) grey correlation degree of T_4, (**e**) grey correlation degree of MCT, (**f**) grey correlation degree of MCT ($\varpi = 0.6$).

6. Conclusions and Future Work

Two main issues related to camera robots with long-span cables are addressed in this paper: MCTDs within the workspace and the CTSA while considering the cable mass.

The MCTDs within the workspace are investigated for the camera robot, and furthermore, the CTSA on the positions of the camera platform is performed. In previous studies, as the author knows, there are few quantitative analyses about MCTDs and the degree of influence of the positions of the camera platform on the cable tensions, in addition to their applications to stability analysis for the camera robot. The following conclusions have been made:

(1) Cable tensions are investigated by a cable tension optimization model for the camera robot with large-span workspaces. Furthermore, the MCTs and MCTDs when the camera platform is located at an arbitrary position within the workspace are presented. The MCT and MCTDs, to the best of our knowledge, are quite different from those in Refs. [17,18], while large-span cables are considered as a catenary model with non-negligible cable mass. Furthermore, the simulation examples depict MCTDs within the workspace. The simulation results of the MCTDs show that when the camera platform of the robot is located in the upper-middle area of the workspace, there are larger MCTs; thus, the cables have stronger constraints on the camera platform, therefore guaranteeing the stability of the camera robot.

(2) A quantitative method for CTSA and a CTSAI for the camera robot is proposed with grey relational analysis; moreover, the CTSA for the camera robot on the positions of the camera platform is analyzed based on numerical simulations and grey relation analysis. It should be pointed that, to the knowledge of the authors, there are few studies in which the CTSA for the cable robots are addressed. It is worth noting that the change laws of the obtained CTSAIs for the four cable tension values and MCTs are consistent with each other. The obtained results for the CTSA of the camera robot show that, with respect to the selected three influencing factors for the cable tensions, the importance has the following sequence: z-direction displacement of the camera platform > x-direction displacement > y-direction displacement. Therefore, the z-direction displacement of the camera platform must be controlled strictly during the operation to accurately control the cable tensions, thereby guaranteeing the stability of the camera robot.

This investigation provides a profound insight into the cable tensions and the influence law of the positions of the camera platform on cable tensions; hence, the investigated MCTDs within the workspace and the proposed CTSA method were examined. In addition, their applications to the stability analysis for the camera robots can be further adopted in other cable robots with large-span cables. Furthermore, further research will be carried out on the experimental verification of the proposed methods and the obtained results in this paper.

Author Contributions: Conceptualization, P.L.; methodology, P.L.; software, P.L.; validation, P.L. and X.Q.; formal analysis, X.Q.; investigation, P.L.; resources, H.T.; data curation, P.L.; writing—original draft preparation, P.L.; writing—review and editing, P.L. and X.Q.; supervision, P.L.; project administration, P.L.; funding acquisition, P.L. and H.T. All authors have read and agreed to the published version of the manuscript.

Funding: This research was funded by the financial support of National Natural Science Foundation of China (NSFC) under Grant No. 52174149, Bilin District Applied Technology Research and Development Projects in 2022 under Grant No. GX2228, and Key Research and Development Program of Shaanxi Province under Grant No. 2022GY-241.

Institutional Review Board Statement: Not applicable.

Informed Consent Statement: Not applicable.

Data Availability Statement: The data used to support the findings of this study are available from the corresponding author upon request.

Acknowledgments: The research is supported by Open Fund of Key Laboratory of Electronic Equipment Structure Design (Ministry of Education) in Xidian University. Moreover, the authors are grateful to the Guest Editor; Bing Li, Wenfu Xu, and Chenglong Fu; and the anonymous reviewers for their constructive comments and helpful suggestions that greatly improved the quality of this article.

Conflicts of Interest: The authors declared no potential conflict of interest with respect to the research, authorship, and/or publication of this article.

References

1. Idà, E.; Mattioni, V. Cable-Driven Parallel Robot Actuators: State of the Art and Novel Servo-Winch Concept. *Actuators* **2022**, *11*, 290. [CrossRef]
2. Luan, P.G.; Thinh, N.T. Wrench-Closure Condition of Cable-Driven Parallel Manipulators. *Appl. Sci.* **2021**, *11*, 4228. [CrossRef]
3. Dinh, T.N.; Park, J.; Park, K.S. Design and evaluation of disturbance observer algorithm for cable-driven parallel robots. *Microsyst. Technol.* **2020**, *26*, 3377–3387. [CrossRef]
4. Zhang, Z.K.; Shao, Z.F.; Wang, L.P. Optimization and implementation of a high-speed 3-DOFs translational cable-driven parallel robot. *Mech. Mach. Theory* **2020**, *145*, 103693. [CrossRef]
5. Venkata Sai Prathyush, I.; Ceccarelli, M.; Russo, M. Control Design for CABLEankle, a Cable Driven Manipulator for Ankle Motion Assistance. *Actuators* **2022**, *11*, 63. [CrossRef]
6. Tho, T.P.; Thinh, N.T. Using a Cable-Driven Parallel Robot with Applications in 3D Concrete Printing. *Appl. Sci.* **2021**, *11*, 563. [CrossRef]
7. Wang, X.G.; Hu, Y.B.; Qi, L. Workspace analysis and verification of cable-driven parallel mechanism for wind tunnel test. *Proc. Inst. Mech. Eng. Part G J. Aerosp. Eng.* **2017**, *231*, 1012–1021. [CrossRef]
8. Deng, S.; Jing, F.; Zheng, R.; Liang, Z.; Yang, G. Multi-objective pose optimal distribution method for the feed support system of Five-hundred-meter Aperture Spherical radio Telescope. *Int. J. Adv. Robot. Syst.* **2018**, *15*, 1729881418756695. [CrossRef]
9. Tang, X.Q. An Overview of the Development for Cable-Driven Parallel Manipulator. *Adv. Mech. Eng.* **2014**, *2014*, 823028. [CrossRef]
10. Su, Y.; Qiu, Y.Y.; Liu, P. The continuity and real-time performance of the cable tension determining for a suspend cable-driven parallel camera robot. *Adv. Robot.* **2015**, *29*, 743–752. [CrossRef]
11. Riehl, N.; Gouttefarde, M.; Krut, S.; Baradat, C.; Pierrot, F. Effects of Non-Negligible Cable Mass on the Static Behavior of Large Workspace Cable-Driven Parallel Mechanisms. In Proceedings of the 2009 IEEE International Conference on Robotics and Automation, Kobe, Japan, 12–17 May 2009; pp. 2193–2198. [CrossRef]
12. Liu, P. On the Mechanics and Stability for the Cable-Driven Parallel Manipulators. Ph.D. Thesis, Xidian University, Xi'an, China, 2015.
13. Hassan, M.; Khajepour, A. Optimization of Actuator Forces in Cable-Based Parallel Manipulators Using Convex Analysis. *IEEE Trans. Robot.* **2008**, *24*, 736–740. [CrossRef]
14. Mikelsons, L.; Bruckmann, T.; Hiller, M.; Schramm, D. A Real-Time Capable Force Calculation Algorithm for Redundant Tendon-Based Parallel Manipulators. In Proceedings of the 2008 IEEE International Conference on Robotics and Automation, Pasadena, CA, USA, 19–23 May 2008; pp. 3869–3874. [CrossRef]
15. Borgstrom, P.H.; Jordan, B.L.; Sukhatme, G.S.; Batalin, M.A.; Kaiser, W.J. Rapid Computation Of Optimally Safe Tension Distributions For Parallel Cable-Driven Robots. *IEEE Trans. Robot.* **2009**, *25*, 1271–1281. [CrossRef]
16. Gosselin, C.; Grenier, M. On the Determination of the Force Distribution in Overconstrained Cable-Driven Parallel Mechanisms. *Meccanica* **2011**, *46*, 3–15. [CrossRef]
17. Liu, P.; Qiu, Y.Y.; Su, Y.; Chang, J. On the Minimum Cable Tensions for the Cable-Based Parallel Robots. *J. Appl. Math.* **2014**, *2014*, 350492. [CrossRef]
18. Liu, P.; Qiu, Y.Y.; Zhang, X.H.; Cao, X.G.; Qiao, X.Z. Minimum Cable Tensions for a Cable-based Parallel Robot with Application to Stability Analysis: A Descriptive Study. *Nov. Res. Asp. Math. Comput. Sci.* **2022**, *2*, 89–101. [CrossRef]
19. Kozak, K.; Zhou, Q.; Wang, J. Static analysis of cable-driven manipulators with non-negligible cable mass. *IEEE Trans. Robot.* **2006**, *22*, 425–433. [CrossRef]
20. Riehl, N.; Gouttefarde, M.; Pierrot, F.; Baradat, C. On the static workspace of large dimensions cable-suspended robots with non-negligible cable mass. In Proceedings of the ASME International Design Engineering Technical Conference, Montreal, QC, Canada, 15–18 August 2010. [CrossRef]
21. Filipovic, M.; Djuric, A.; Kevac, L. Contribution to the modeling of cable-suspended parallel robot hanged on the four points. In Proceedings of the 2012 IEEE/RSJ International Conference on Intelligent Robots and Systems, Vilamoura-Algarve, Portugal, 7–12 October 2012; pp. 3526–3531. [CrossRef]
22. Merlet, J.P.; Tissot, R. A panorama of methods for dealing with sagging cables in cable driven parallel robots. In *Advances in Robot Kinematics 2022. ARK 2022*; Springer Proceedings in Advanced Robotics; Altuzarra, O., Kecskeméthy, A., Eds.; Springer: Cham, Switzerland, 2022; Volume 24. [CrossRef]
23. Merlet, J.P. The Forward Kinematics of the 4-1 Cable-Driven Parallel Robot with Non Elastic Sagging Cables. In *Advances in Robot Kinematics 2020. ARK 2020*; Springer Proceedings in Advanced Robotics; Lenarčič, J., Siciliano, B., Eds.; Springer: Cham, Switzerland, 2021; Volume 15. [CrossRef]
24. Jung, J. Workspace and Stiffness Analysis of 3D Printing Cable-Driven Parallel Robot with a Retractable Beam-Type End-Effector. *Robotics* **2020**, *9*, 65. [CrossRef]
25. Heo, J.-M.; Park, B.-J.; Park, J.-O.; Kim, C.-S.; Jung, J.; Park, K.-S. Workspace and stability analysis of a 6-DOF cable-driven parallel robot using frequency-based variable constraints. *J. Mech. Sci. Technol.* **2018**, *32*, 1345–1356. [CrossRef]

26. Pott, A. Influence of pulley kinematics on cable-driven parallel robots. In *Latest Advances in Robot Kinematics*; Lenarcic, J., Husty, M., Eds.; Springer: Dordrecht, The Netherlands, 2012; pp. 197–204. [CrossRef]
27. Idà, E.; Carricato, M. A new performance index for underactuated cable-driven parallel robots. In *Cable-Driven Parallel Robots*; Gouttefarde, M., Bruckmann, T., Pott, A., Eds.; Springer International Publishing: Cham, Switzerland, 2021; Volume 104, pp. 24–36. [CrossRef]
28. Mottola, G.; Gosselin, C.; Carricato, M. Effect of actuation errors on a purely-translational spatial cable-driven parallel robot. In Proceedings of the 2019 IEEE 9th Annual International Conference on CYBER Technology in Automation, Control, and Intelligent Systems (CYBER), Suzhou, China, 29 July–2 August 2019; pp. 701–707.
29. Mattioni, V.; Idà, E.; Carricato, M. Force-distribution sensitivity to cable-tension errors in overconstrained cable-driven parallel robots. *Mech. Mach. Theory* **2022**, *175*, 104940. [CrossRef]
30. Mattioni, V.; Idà, E.; Carricato, M. Force-distribution sensitivity to cable-tension errors: A preliminary investigation. In *Cable-Driven Parallel Robots*; Gouttefarde, M., Bruckmann, T., Pott, A., Eds.; Springer International Publishing: Cham, Switzerland, 2021; Volume 104, pp. 129–141. [CrossRef]
31. Chen, Q.L.; Lin, Q.; Wei, G.W.; Ren, L. Tension vector and structure matrix associated force sensitivity of a 6-DOF cable-driven parallel robot. *Proc. Inst. Mech. Eng. C* **2022**, *236*, 100–114. [CrossRef]
32. Wu, D.F.; Wang, N.L.; Yang, Z.P.; Li, C.Z.; Yang, Y.P. Comprehensive Evaluation of Coal-Fired Power Units Using Grey Relational Analysis and a Hybrid Entropy-Based Weighting Method. *Entropy* **2018**, *20*, 215. [CrossRef] [PubMed]
33. Liu, P.; Qiao, X.Z.; Zhang, X.H. Stability sensitivity for a cable-based coal-gangue picking robot based on grey relational analysis. *Int. J. Adv. Robot. Syst.* **2021**, *18*, 17298814211059729. [CrossRef]
34. Liu, P.; Tian, H.B.; Cao, X.G.; Zhang, X.H.; Qiao, X.Z.; Su, Y. Dynamic Stability Measurement and Grey Relational Stability Sensitivity Analysis Methods for High-Speed Long-Span 4-1 Cable Robots. *Mathematics* **2022**, *10*, 4653. [CrossRef]
35. Liu, S.F.; Forrest, J. The current developing status on grey system theory. *J. Grey Syst.* **2007**, *19*, 111–123.
36. Liu, S.F.; Xie, N.M.; Forrest, J. On new models of grey incidence analysis based on visual angle of similarity and nearness. *Syst. Eng.-Theory Pract.* **2010**, *30*, 881–887.
37. Deng, J.L. Control problems of grey systems. *Syst. Control Lett.* **1982**, *5*, 288–294.
38. Wang, W.P.; Yang, Z.M.; Lu, Y.; Shi, Y.; Zhang, B. The Optimization Degree of Provincial Industrial Ecosystem and EKC of China-Based on the Grey Correlation Analysis. *J. Grey Syst.* **2016**, *28*, 1–12.
39. Diba, S.; Xie, N.M. Sustainable supplier selection for Satrec Vitalait Milk Company in Senegal using the novel grey relational analysis method. *Grey Syst. Theory Appl.* **2019**, *9*, 262–294. [CrossRef]
40. Wang, X.N.; Yang, W.C.; Ge, Y.; Feng, D. The influence of shrinkage-reducing agent solution properties on shrinkage of cementitious composite using grey correlation analysis. *Constr. Build. Mater.* **2020**, *264*, 120194. [CrossRef]
41. Li, J.; Li, X.; Lv, N.; Yang, Y.; Xi, B.; Li, M.; Bai, S.; Liu, D. Quantitative assessment of groundwater pollution intensity on typical contaminated sites in China using grey relational analysis and numerical simulation. *Environ. Earth Sci.* **2015**, *74*, 3955–3968. [CrossRef]
42. Liu, S.F.; Dang, Y.G.; Fang, Z.F. *Grey System Theory and Its Application*; Science Press: Beijing, China, 2021.
43. Xiao, X.P. Theoretical Study and Reviews on the Computation Method of Grey Interconnet Degree. *Syst. Eng.-Theory Pract.* **1997**, *8*, 77–82.
44. Irivne, H.M. *Cable Structures*; MIT Press: Cambridge, MA, USA, 1981; pp. 16–20.
45. Du, J.L.; Duan, X.C.; Bao, H. Static Stiffness of a Cable-supporting System with the Cable Sags Effects Considered. *J. Mech. Eng.* **2010**, *46*, 29–34. [CrossRef]
46. Gouttefarde, M.; Collard, J.F.; Riehl, N.; Baradat, C. Simplified Static Analysis of Large-Dimension Parallel Cable-Driven Robots. In Proceedings of the IEEE International Conference on Robotics and Automation River Centre, Saint Paul, MN, USA, 14–18 May 2012; pp. 2299–2305. [CrossRef]
47. Su, Y.; Qiu, Y.Y.; Liu, P. Optimal Cable Tension Distribution of the High-Speed Redundant Driven Camera Robots Considering Cable Sag and Inertia Effects. *Adv. Mech. Eng.* **2014**, *6*, 729020. [CrossRef]
48. Idá, E.; Briot, S.; Carricato, M. Identification of the inertial parameters of underactuated Cable-Driven Parallel Robots. *Mech. Mach. Theory* **2022**, *167*, 104504. [CrossRef]
49. Liu, P.; Qiu, Y.Y. Tension Optimization for a Cable-Driven Parallel Robot with Non- Negligible Cable Mass. *Open Autom. Control Syst. J.* **2015**, *7*, 1973–1980. [CrossRef]
50. Idá, E.; Briot, S.; Carricato, M. Natural Oscillations of Underactuated Cable-Driven Parallel Robots. *IEEE Access* **2021**, *9*, 71660–71672. [CrossRef]
51. Liu, P.; Tian, H.; Cao, X.; Qiao, X.; Gong, L.; Duan, X.; Qiu, Y.; Su, Y. Pick–and–Place Trajectory Planning and Robust Adaptive Fuzzy Tracking Control for Cable–Based Gangue–Sorting Robots with Model Uncertainties and External Disturbances. *Machines* **2022**, *10*, 714. [CrossRef]
52. Beer, F.P.; Johnston, E.R., Jr.; DeWolf, J.T.; Mazurek, D.F. *Mechanics of Materials*; McGraw-Hill: New York, NY, USA, 2012.
53. He, X.; Li, L.; Liu, X.; Wu, Y.; Mei, S.; Zhang, Z. Using grey relational analysis to analyze influential factor of hand, foot and mouth disease in Shenzhen. *Grey Syst.-Theory Appl.* **2019**, *9*, 197–206. [CrossRef]

54. Zhang, C.; Duan, L.; Liu, H.; Zhang, Y.; Yin, L.; Lu, Q.; Duan, G. Identifying the Influencing Factors of Patient's Attitude to Medical Service Price by Combing Grey Relational Theory with CMH Statistical Analysis. *J. Grey Syst.* **2020**, *32*, 80–95.
55. Hu, Y.-C.; Jiang, P.; Chiu, Y.-J.; Ken, Y.-W. Incorporating Grey Relational Analysis into Grey Prediction Models to Forecast the Demand for Magnesium Materials. *Cybern. Syst.* **2021**, *52*, 522–532. [CrossRef]